Bladder wall flattening with conformal mapping for MR cystography

Ruirui Jiang*[a], Hongbin Zhu[b], Wei Zeng[a], Xiaokang Yu[a], Yi Fan[b], Xianfeng Gu[a], and Zhengrong Liang[a,b]
[a] Departments of Computer Science, State University of New York, NY, USA 11790;
[b] Departments of Radiology, State University of New York, NY, USA 11790

ABSTRACT

Magnetic resonance visual cystoscopy or MR cystography (MRC) is an emerging tool for bladder tumor detection, and 3D endoscopic views on the inner bladder surface are being investigated by researchers. In this paper, we further investigate an innovative strategy of visualizing the inner surface by flattening the 3D surface into a 2D display, where conformal mapping, a mathematically-proved algorithm with shape preserving, is used. The original morphological, textural and even geometric information can be visualized in the flattened 2D image. Therefore, radiologists do not have to manually control the view point and angle to locate the possible abnormalities like what they do in the 3D endoscopic views. Once an abnormality is detected on the 2D flattened image, its locations in the original MR slice images and in the 3D endoscopic views can be retrieved since the conformal mapping is an invertible transformation. In such a manner, the reading time needed by a radiologist can be expected to be reduced. In addition to the surface information, the bladder wall thickness can be visualized with encoded colors on the flattened image. A normal volunteer and a patient studies were performed to test the reconstruction of 3D surface, the conformal flattening, and the visualization of the color-coded flattened image. A bladder tumor of 3 cm size is so obvious on the 2D flattened image such that it can be perceived only at the first sight. The patient dataset shows a noticeable difference on the wall thickness distribution than that of the volunteer's dataset.

Keywords: Virtual cystoscopy, bladder tumor, MR images, conformal mapping, harmonic map, flattening, bladder wall thickness

1. INTRODUCTION

Bladder cancer is the fifth leading cause of cancer deaths in the United States[1], and each year, bladder tumor is diagnosed in more than 50,000 subjects according to American Cancer Society. Optical cystoscopy is widely used to accurately evaluate the entire bladder, and to help early diagnosis and proper treatment of bladder carcinoma, despite the fact that it is invasive and expensive. In the past few years, virtual cystoscopy (VCys) has been under development for an alternative non-invasive means to exam virtually the entire bladder[2]. Compared to Computed Tomography (CT) technology used in most previous VCys work, Magnetic Resonance visual cystoscopy or MR cystography (MRC) has the advantage of not delivering excessive X-ray exposure, which makes it a possible substitute. Therefore, MR imaging (MRI) has recently received attentions from both researchers and physicians, for its safety to the patients, and structural and functional information for diagnosing and staging the tumor growth[3].

In MRC, a patient is scanned by a MR device with bladder extended with urine. Then two-dimensional (2D) MR slice images are acquired and the 3D inner surface of the bladder wall in the images is routinely examined by radiologists in 2D slice displays. Such process is often time consuming and wearing, and even leads to fatigue error in bladder evaluation and diagnosis. Thus, 3D endoscopic views on the inner surface are investigated and developed, where a 3D model is reconstructed for quick detection. However, since inner and outer surfaces of the bladder wall are both topological sphere-like, it still takes time to fully examine the bladder wall in order to find suspicious regions. Therefore, for purpose of quick detections, algorithms for flattening the 3D model to a 2D image while retaining necessary pathological information are highly desired.

In this work, we build a framework of reconstructing the 3D bladder data from the MR images. Then a segmentation algorithm is applied to acquire the inner bladder surface information. With that information, we use the conformal mapping algorithm to flatten the 3D surface to a 2D image. During that process, the geometric information of the

*jiang@cs.sunysb.edu; phone 1 631 444-2736

original surface is retained as far as possible. Furthermore, bladder wall thickness calculation algorithm for visualizing the wall thickness characteristics is also utilized to improve the detection and examination[4].

The rest of the paper is organized as follows. In Section 2, we explain our framework of visualizing bladder walls in details. The theory and algorithm of each step are illustrated. Experimental results are reported in Section 3. Finally in Section 4, we summarize our work with a sketch of future plan.

2. METHODS

We firstly acquire the T1-weighted MR images of the bladder, where the urine signal is attenuated for good contrast against the wall, and then apply an automated segmentation algorithm to find the inner and outer surfaces of the bladder wall in the images. The segmented inner surface is flattened by conformal mapping to preserve the surface geometry. Both the inner and outer surfaces are used to calculate the wall thickness. The thickness distribution of the bladder wall is visualized by colors in the flattened image. The methods to be presented in this paper are based on four steps: (1) acquisition of the raw and segmented volume image data, (2) calculation of the bladder wall thickness, (3) conformal mapping of the inner surface to a sphere, and (4) visualization of the 3D inner surface and the color-coded flattened image. These four steps are described below.

2.1 Acquisition of the raw and segmented volume image data

We choose T1-weighted MR imaging instead of T2-weighted images used in many previous work for two reasons. On one hand, the image intensities of urine is decreased in T1-weighted images, which provides good contrast between the bladder wall and lumen. On the other hand, the partial volume effect in T1-weighted image is less visible.

From the acquired T1-weighted bladder images in DICOM format, we resample the image voxel sizes and build the corresponding raw volume, where each voxel in the sampled volume is a cubic element. Then we clip the raw volume, only keeping the bladder and its surrounding area. This can significantly reduce the work of automatic segmentation.

A coupled level set based segmentation algorithm[5] is applied to the sampled raw volume to classify each voxel to one of the three types: the urine inside the bladder, the bladder wall, and the tissues outside the bladder. The algorithm gets an initial guess from modified Chan-Vese (CV) model, then uses the level set method on both the inner and outer borders iteratively. The segmentation result shows improvement compared to the well-known CV model.

2.2 Calculation of bladder wall thickness

We are developing an efficient algorithm based on electric field to calculate the bladder wall thickness[6]. From the segmentation result, we get the inner and outer surfaces, which are represented by the innermost and outermost voxels of the segmented bladder wall, respectively. The inner and outer surfaces are closed surfaces which do not intersect with each other. We assume that the inner surface has an electric potential 0, while the outer one has a potential 1. Then an electric field between the inner and outer surfaces can be constructed. From each voxel on the inner surface, we travel along the gradient direction until we reach the outer surface. In the process, we integrate along the path to calculate its length, and get the wall thickness of that voxel.

There are alternative methods to calculate the thickness. For example, for each vertex on the inner surface, we can simply find the nearest vertex on the outer surface, and then calculate their Euclidean distance[7]. This method has its advantage in running time. However, it may not generate a reasonable result when the inner surface is concave.

2.3 Conformal mapping of the inner surface to a sphere

2.3.1 Basis of conformal mapping

It is well known in mathematics that any closed genus zero surface can be mapped conformally (angle-preserving) onto the unit sphere[8]. The mapping is a diffeomorphism. Two such conformal mappings differ by a Möbius transformation on the sphere. All Möbius transformations form a six-dimensional group. Furthermore, any harmonic map from the genus zero closed surface to the unit sphere is conformal. Conformal mapping has been successfully applied in brain surface mapping[9]. Here we first introduce its theoretical background.

Suppose $\mathbf{r}(u,v)$ is a surface embedded in the three dimensional Euclidean space $\mathbb{R}^3$, where (u,v) are local parameters. We use $\mathbf{r}_u$ to denote $\frac{\partial \mathbf{r}}{\partial u}$, and $\mathbf{r}_v$ to denote $\frac{\partial \mathbf{r}}{\partial v}$. The parameters are regular if $\mathbf{r}_u \times \mathbf{r}_v \neq 0$. We assume (u,v) are regular parameters.

Let $d\mathbf{r} = \mathbf{r}_u du + \mathbf{r}_v dv$ be a tangent vector of the surface, the norm of the vector in $\mathbb{R}^3$ is given by

$$< d\mathbf{r}, d\mathbf{r} >= \begin{pmatrix} du & dv \end{pmatrix} \begin{pmatrix} E(u,v) & F(u,v) \\ F(u,v) & G(u,v) \end{pmatrix} \begin{pmatrix} du \\ dv \end{pmatrix} \tag{1}$$

where $E(u,v) =< \mathbf{r}_u, \mathbf{r}_u >$, $F(u,v) =< \mathbf{r}_u, \mathbf{r}_v >$ and $G(u,v) =< \mathbf{r}_v, \mathbf{r}_v >$. Then the matrix

$$\mathbf{g}(u,v) = \begin{pmatrix} E(u,v) & F(u,v) \\ F(u,v) & G(u,v) \end{pmatrix} \tag{2}$$

defines an inner product on the tangent plane at $\mathbf{r}(u,v)$, which is called a *Riemannian metric tensor* of the surface. The tangent vector length and the angle can be measured by the Riemannian metric $\mathbf{g}$. Let $(\tilde{u}, \tilde{v})$ be another local parameter of the same surface, and let the Jacobi matrix be

$$J = \begin{pmatrix} \frac{\partial \tilde{u}}{\partial u} & \frac{\partial \tilde{u}}{\partial v} \\ \frac{\partial \tilde{v}}{\partial u} & \frac{\partial \tilde{v}}{\partial v} \end{pmatrix} \tag{3}$$

Then the matrix tensor on $(\tilde{u}, \tilde{v})$ is

$$\begin{pmatrix} E & F \\ F & G \end{pmatrix} = J^{T} \begin{pmatrix} \tilde{E} & \tilde{F} \\ \tilde{F} & \tilde{G} \end{pmatrix} J \tag{4}$$

Let $d\mathbf{r} = \mathbf{r}_u du + \mathbf{r}_v dv$ and $\delta\mathbf{r} = \mathbf{r}_u \delta u + \mathbf{r}_v \delta v$ be two tangent vectors, then the angle between the two vectors are θ, then

$$\cos\theta = \frac{< d\mathbf{r}, \delta\mathbf{r} >_{\mathbf{g}}}{\sqrt{< d\mathbf{r}, d\mathbf{r} >_{\mathbf{g}}}\sqrt{< \delta\mathbf{r}, \delta\mathbf{r} >_{\mathbf{g}}}} \tag{5}$$

Suppose $\mathbf{g}_1$ and $\mathbf{g}_2$ are two Riemannian metrics on the same surface, and

$$\mathbf{g}_2 = e^{2\lambda(u,v)}\mathbf{g}_1. \tag{6}$$

By Equation 5, it can be verified that the angles between $d\mathbf{r}$ and $\delta\mathbf{r}$ measured by $\mathbf{g}_1$ and $\mathbf{g}_2$ are equal. Therefore we say $\mathbf{g}_1$ and $\mathbf{g}_2$ are *conformal*, namely, *angle preserving*.

Suppose $f : (M, \mathbf{g}) \to (N, \mathbf{h})$ is a differential map between two surfaces M and N. $\mathbf{g} = (g_{ij})$ and $\mathbf{h} = (h_{ij})$ be the Riemannian metrics of M and N respectively. Assume (x,y) and (u,v) be the local parameters of M and N respectively, then the map f has local representation $(u(x,y), v(x,y))$. f maps a tangent vector (dx, dy) of M to the tangent vector (du, dv) on N, and we define the length of (dx, dy) as that of (du, dv). This defines metric on M, which is called the *pull back metric* induced by f,

$$f^*\mathbf{h} = J^T \mathbf{h} J, \tag{7}$$

where J is the Jacobi matrix

$$J = \begin{pmatrix} \frac{\partial u}{\partial x} & \frac{\partial u}{\partial y} \\ \frac{\partial v}{\partial x} & \frac{\partial v}{\partial y} \end{pmatrix}. \tag{8}$$

If the pullback metric $f^*\mathbf{h}$ on M is conformal to the original metric $\mathbf{g}$,

$$\mathbf{g} = e^{2\lambda(x,y)} f^*\mathbf{h}, \tag{9}$$

then the map f is a *conformal map*. Intuitively, a conformal map preserves angles.

Suppose $\mathbb{S}^2$ be the unit sphere $x^2 + y^2 + z^2 = 1$, then the stereographic projection $\phi : \mathbb{S}^2 \to \mathbb{C}$ maps the sphere to the complex plane, $(x,y,z) -> u + iv$,

$$(u,v) = (\frac{x}{1-z}, \frac{y}{1-z}), \tag{10}$$

which is conformal. All the conformal maps from the whole complex plane to itself are given by the so-called Möbius transformations:

$$\tau(z) = \frac{az+b}{cz+d}, ad-bc = 1, a, b, c, d \in \mathbb{C}. \tag{11}$$

Then composition $\phi^{-1} \circ \tau \circ \phi : \mathbb{S}^2 \to \mathbb{S}$ is a spherical conformal map, namely a spherical Möbius transformation. It is easy to see that all the Möbius transformations form a 6 dimensional group.

All genus zero closed metric surface can be conformally mapped to the unit sphere. The conformal mappings are not unique. Two such mappings differ by a spherical Möbius transformation.

Let $(M, \mathbf{g})$ and $(N, \mathbf{h})$ be surfaces with Riemannian metrics $\mathbf{g}$ and $\mathbf{h}$ respectively, and let f be a C^1 map from M to N. The *harmonic energy density* is given by

$$|df|^2 = \sum_{i,j,\alpha,\beta} g^{\alpha\beta}(x,y) h_{ij}(u(x)) \frac{\partial u^i}{\partial x^\alpha} \frac{\partial u^j}{\partial x^\beta} \tag{12}$$

where $(g^{\alpha\beta})$ is the inverse matrix of $\mathbf{g} = (g_{ij})$. The *harmonic energy* of the map is given by

$$E(f) = \int_M |df|^2 dv_M, \tag{13}$$

where $dv_M = \sqrt{det(\mathbf{g})}dx$ is the area element of M. The critical points of E is the space of maps are called *harmonic maps*. The following theorem plays a fundamental role in our current work:

For closed zero closed metric surfaces, degree one harmonic maps are conformal maps.

If the target surface $N = \mathbb{R}^3$, $h_{ij} = \delta_{ij}$, and $f = (f_1, f_2, f_3)$, then the harmonic energy has a simpler form

$$E(f) = \sum_{i=1}^{3} \int_M |\nabla f_i|^2 dv_M, \tag{14}$$

where ∇f_i is the gradient of $f_i : M \to \mathbb{R}$,

$$\nabla f_i = \begin{pmatrix} g^{11} & g^{12} \\ g^{21} & g^{22} \end{pmatrix} \begin{pmatrix} \frac{\partial f_i}{\partial x^1} \\ \frac{\partial f_i}{\partial x^2} \end{pmatrix} \tag{15}$$

Harmonic maps satisfy the following Laplace equation

$$\Delta f_i = 0, i = 1, 2, 3. \tag{16}$$

where Δ is the Laplace-Beltrami operator on M. It has the local representation

$$\Delta f = \frac{1}{\sqrt{det(\mathbf{g})}} \frac{\partial}{\partial x^i} (\sqrt{det(\mathbf{g})} g^{ij} \frac{\partial}{\partial x^j} f). \tag{17}$$

The harmonic map can be constructed by *diffusion method*. Let $f(t) : M \to \mathbb{S}^2$ be C^1 maps from a genus zero closed metric surface to the unit sphere, such that $f(0)$ is a degree one map, such as the *Gauss map*,

$$G(p) = \mathbf{n}(p), \forall p \in M, \tag{18}$$

where $\mathbf{n}(p)$ is the unit normal vector at point$p$. The heat diffusion is given by

$$\frac{\partial f_i(p,t)}{\partial t} = -\Delta_p f_i(p,t), \tag{19}$$

then $f(t)$ will converge to a harmonic map under the following normalization condition,

$$\int_M f(p,t) \equiv \mathbf{0}. \tag{20}$$

In practice, the surfaces are approximated by polyhedral surfaces, especially triangle meshes, where each face is a Euclidean triangle. A triangle mesh is a simplicial complex. We use v_i to denote a vertex, $[v_i, v_j]$the edge connecting v_i andv_j; $[v_i, v_j, v_k]$ a triangle face connecting three vertices.

A function f is approximated by a piecewise linear function. Suppose $\sigma = [v_0, v_1, v_2]$ is one triangle, then any point $v \in \sigma$ can be represented as

$$v = \alpha v_0 + \beta v_1 + \gamma v_2, \alpha, \beta, \gamma > 0, \alpha + \beta + \gamma = 1. \tag{21}$$

Suppose f is a piecewise linear function $f : \sigma \to \mathbb{R}$, then

$$f(v) = \alpha f(v_0) + \beta f(v_1) + \gamma f(v_2). \tag{22}$$

By direct computation, the harmonic energy of f on the face σ is given by

$$E(f|_\sigma) = \cot\theta_0(f(v_1) - f(v_2))^2 + \cot\theta_1(f(v_2) - f(v_0))^2 + \cot\theta_2(f(v_0) - f(v_1))^2. \tag{23}$$

Similarly, the harmonic energy of f defined on the whole mesh M is given by

$$E(f) = \sum_{[v_i,v_j]} w_{ij}(f(v_i) - f(v_j))^2, \tag{24}$$

where w_{ij} is the edge weight

$$w_{ij} = \cot\theta_{ij}^k + \cot\theta_{ij}^l, \tag{25}$$

θ_{ij}^k and θ_{ij}^l are the two angles against the edge $[v_i, v_j]$.

The discrete Laplace-Beltrami operator is given by

$$\Delta f(v_i) = \sum_{[v_i,v_j]} w_{ij}(f(v_i) - f(v_j)). \tag{26}$$

2.3.2 Computational algorithms

Since our conformal mapping algorithm is based on triangle mesh, we utilize marching cube algorithm[10] to generate the triangle mesh of the inner surface from the segmented volume data. Ideally, the algorithm outputs topological sphere, i.e., genus 0 closed surface, which will be conformally mapped to a sphere later.

Then a half-edge data structure to represent the triangle mesh is built upon the result of the marching cube algorithm. This data structure, in which the connection of faces, edges and vertices of the triangle mesh is constructed and visited efficiently, is widely used in geometric modeling and other fields.

After that, the normal vector of each vertex of the mesh is calculated. And for each vertex, we get its thickness from the pre-calculated thickness value of the voxel in which it lies. Those two kinds of information will be useful in the visualization part.

Now we are ready to map the bladder inner wall to a sphere. Our algorithm is based on the nonlinear heat diffusion method. We first find a degree one map $\vec{f}$ between the inner wall surface M and the unit sphere S^2. The map may not be a diffeomorphism, and will be smoothed out automatically during the process. We evolve $\vec{f}$ to minimize its harmonic energy until it becomes a harmonic map. The evolution is according to a nonlinear heat diffusion process

$$\frac{d\vec{f}(t)}{dt} = -\Delta\vec{f}(t),$$

where Δ is the Laplace-Beltrami operator on the surface determined by its induced Euclidean metric. Since $\vec{f}(M)$ is constrained to be on the unit sphere, we need to project $-\Delta\vec{f}$ onto the tangent space of the sphere.

The algorithm is described below: input: mesh M, step length δt, energy difference threshold δE; output: a harmonic map $\vec{f} : M \to \mathrm{S}^2$, which satisfies the zero mass-center constraint.

1) Compute Gauss map $N : M \to \mathrm{S}^2$. Let $\vec{f} = N$, compute harmonic energy E_0.

2) For each vertex $v \in M$, compute the Laplacian, project it to the tangent space to get $\Delta\vec{f}$.

3) Update $\vec{f}$ by $\delta\vec{f} = -\Delta\vec{f}\delta t$.

4) Normalize the map, such that the mass center of $\vec{f}(M)$ is at the origin.

5) If $|E - E_0| < \delta E$, return $\vec{f}$. Otherwise, assign E to E_0 and repeat steps 2)-5).

By choosing the step length carefully, the energy can be decreased monotonically during the process.

2.4 Visualization

In the previous step, we map the inner bladder wall to a sphere, with thickness value and normal vector attached on each vertex. Here, we firstly do a thickness mapping to transfer the value to a color so that we can visualize them, and find thick or abnormal regions quickly. Then we offer two options to map the sphere to 2D plane – pole projection and earth map. Finally the result is shown on the screen with graphics techniques.

2.4.1 Color mapping

We use a simple linear method to encode colors. Firstly each thickness value is normalized to a real number between 0 and 1. To further make the major parts of different bladders look similar in color, we reset the median thickness value to 0.5, and the distribution of larger and smaller values are rescaled accordingly. After that, we assign six basic colors: red, yellow, green, cyan, blue, and purple, to thickness 1, 0.8, 0.6, 0.4, 0.2, and 0, respectively. If a thickness value is between two values listed above, we linearly interpolate the three RGB channels of two corresponding basic colors to get the three channels of the color of the specific thickness value.

2.4.2 Flattening of the mapped sphere

We have two ways of flattening the sphere: (1) to two unit disks, and (2) to an ellipse on the plane. The first method is based on stereographic projection. For the lower hemisphere, we use north pole as the projection center. Each vertex of the hemisphere is mapped to the intersection of the line connecting the north pole and itself, and the equator plane. For the upper hemisphere, we do the same thing, but use south pole as the projection center instead.

The second method is based on Mollweide projection, which is well studied in cartography, and widely used for global maps[11]. The projection is:

$$x = \frac{2\sqrt{2}}{\pi}\lambda\cos\theta, \qquad y = \sqrt{2}\sin\theta, \tag{27}$$

where θ is an angle defined by $2\theta + \sin 2\theta = \pi\sin\phi$. Here λ is the longitude from the central meridian, and ϕ is the latitude.

Both methods have their own merits. The earth map can show the result in only one picture, but it has higher distortion in the north and south poles.

2.4.3 OpenGL rendering

We employ OpenGL to visualize the results. The normal vector of each vertex is set to the attached values on each vertex of the original bladder surface mesh, and the vertex colors are just calculated from color mapping. OpenGL can render the result meshes with colors smoothly and automatically.

3. RESULTS

We tested the whole pipeline on nine bladder datasets on a computer with Intel Xeon 3.4G CPU and 3GB RAM. For each dataset, the volume size is about 180×180×180, and the number of vertices of the triangle mesh is about 50,000. In the framework, each of the first three steps described in the previous section takes about 20 minutes, so it takes approximately one hour for each dataset. The results are shown by the figures below and consistent with expectations.

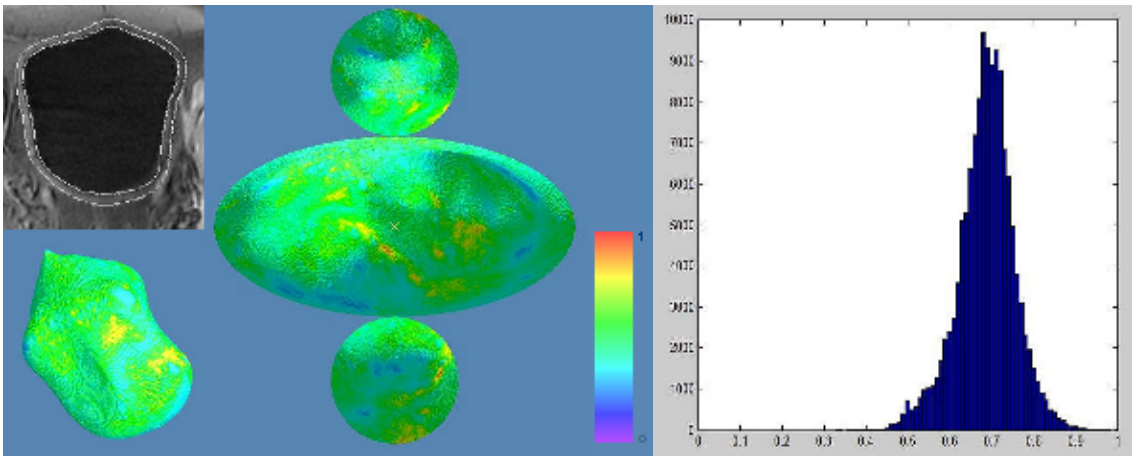

Figure 1: Result of the first data set. Left up – one slice of the raw data with segmentation result. Left down – bladder inner surface. Middle – flattened two disks and ellipse. The color bar indicates the color mapping of the normalized bladder wall thickness. Red color stands for larger value than violet. Right – the histogram of thickness value distribution.

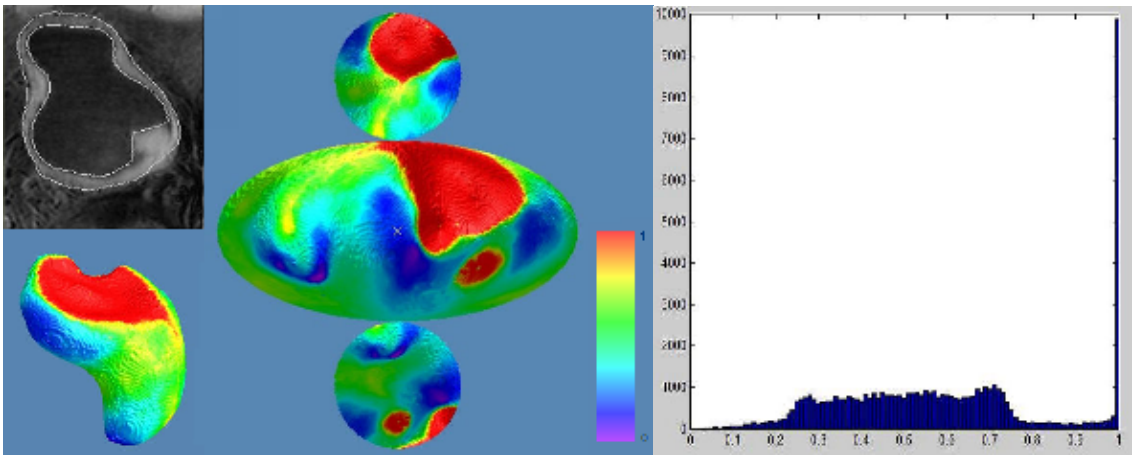

Figure 2: Result of the third data set. Note that there is a straight line on the right (with thickness value 1) in the histogram, which also contributes to the large red area on the bladder

.

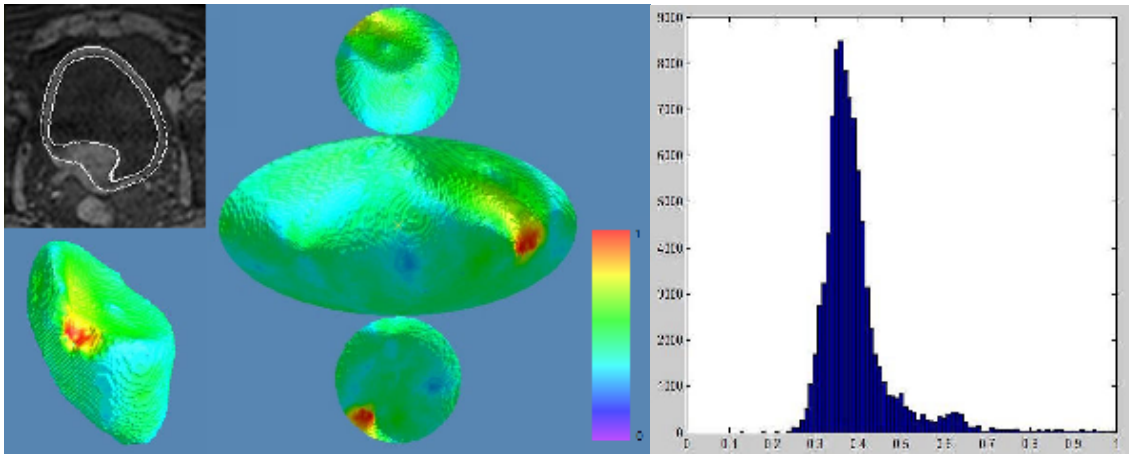

Figure 3: Result of the fifth data set.

We pick the 1st, 3rd, and 5th dataset to illustrate. The slices and flattened results coincide with each other in all of the three cases, and strongly support our guess that the 1st bladder is healthy, while the other two have tumors.

The results also show that the segmentation algorithm works well generally. Sometimes (5 out of 9 cases in our running), the algorithm generates some (from 1 to 4) tiny pieces at the same time, due to the survived noises in the segmented data. However, these pieces are isolated from the bladder wall, and can be easily removed by simply picking the largest connecting component of the segmented data.

4. CONCLUSION

In this study, we presented an integrated pipeline to process T1-weighted MR bladder images and to accelerate the evaluation of the entire bladder. The conformal mapping algorithm and the thickness calculation algorithm offer us a fast way to detect the regions in the bladder with abnormal thickness. The innovations reside in this study consist of (1) a systematic method for bladder wall reconstruction and flattening; (2) an efficient algorithm for calculating bladder wall thickness; and (3) an innovative way to visualize the entire bladder wall. These innovations enable us to visualize the bladder wall geometry and the wall thickness characteristics, and reduce the complexity from 3D to 2D operation.

In our future work, we will further improve the segmentation algorithm and visualization quality, and try to minimize the information loss and inaccuracy in each step of the pipeline. The applications in Computer Aided Detection (CAD) are also under progress.

ACKNOWLEDGEMENT

This work was partly supported by NIH Grant #CA120917 and #CA082402 of the National Cancer Institute, NSFC 60628202 and NSF IIS-0713145. The authors would appreciate the assistance of Dr. Chris Lee, Dr. Mark Wagshul and Ms. Aimee Minton on data acquisition.

REFERENCES

[1] A. Jemal, A. Thomas, T. Murray, and M. Thun, "Cancer statistics," A Cancer Journal for Clinicians, 52, 23-47, 2002.

[2] D.J. Vining, R.J. Zagoria, K. Liu, and D. Stelts, "CT cystoscopy: an innovation in bladder imaging," American Journal of Roentgenology, 166, 409-410, 1996.
[3] Li, L., Wang, Z., and Liang, Z., "Bladder Cancer Screening by Magnetic Resonance Imaging," in The Handbook of Cancer Models with Applications to Cancer Screening, Cancer Treatment and Risk Assessment, pp. 457–470 (2008).
[4] Z. Liang, D. Chen, T. Button, H. Li, and W. Huang, "Feasibility studies on extracting bladder wall from MR images for virtual cystoscopy," Proc. International Society of Magnetic Resonance in Medicine, 3, 2204, 1999.
[5] Duan,C., Liang, Z., et al., "A coupled level-set framework for bladder wall segmentation with application to MRI-based virtual cystoscopy," accepted by IEEE Transactions on Medical Imaging.
[6] Zhu, H., et al., "Computer-aided detection of bladder tumors based on the thickness mapping of bladder wall in MR images," accepted by SPIE Medical Imaging 2010.
[7] Jaume, S., Ferrant, M., Macq, B., Schreyer, A., Kikinis, R., and Warfield, S. K., "Tumor detection in the bladder wall with a measurement of abnormal thickness in ct scans," IEEE Transactions on Biomedical Engineering 50, 383–390 (2003).
[8] Gu, X. and Yau, S.-T., [Computational Conformal Geometry], Higher Education Press, Beijing, China (2008).
[9] Gu, X., Wang, Y., Chan, T. F., Thompson, P. M., and Yau, S.-T., "Genus zero surface conformal mapping and its application to brain surface mapping," IEEE Transactions on Medical Imaging, vol. 23, 949–958 (2004).
[10] Lorensen WE, Cline HE: "Marching cubes: A high resolution 3D surface construction algorithm," Computer Graphics. 21(4): 163-169 (1987)
[11] Snyder, J., [Map Projections - A Working Manual], United States Government Printing, Washington, DC (1983).